1,10-Phenanthrolines with Tunable Luminescence upon Protonation: A Spectroscopic and Computational Study

Andrea Listorti,[†] Alessandra Degli Esposti,[†] Ravuri S. K. Kishore,[‡] Venkateshwarlu Kalsani,[‡] Michael Schmittel,*[,‡] and Nicola Armaroli*[,†]

Center of Micro and Nanochemistry and Engineering, Organische Chemie I, Universität Siegen, Adolf-Reichwein-Strasse, D-57068 Siegen, Germany, and Molecular Photoscience Group, Istituto per la Sintesi Organica e la Fotoreattività, Consiglio Nazionale delle Ricerche, Via Gobetti 101, 40129 Bologna, Italy

Received: March 26, 2007; In Final Form: May 16, 2007

We have synthesized nine 2,9-aryl-substituted 1,10-phenanthrolines (**1**−**9**) with the aim of rationalizing their electronic absorption and luminescence properties in both the basic and acid form. The latter are generated upon addition of trifluoroacetic acid to CH_2Cl_2 solutions of **1**−**9** and their formation is unambiguously evidenced by UV−vis absorption and ^{1}H NMR spectroscopy. **1**−**9** can be subdivided into three groups, depending on their chemical structure and luminescence behavior. **1**−**3** are symmetrically substituted *p*-dianisylphenanthrolines which exhibit relatively intense violet fluorescence in CH_2Cl_2 (λ_{max} ca. 400 nm, $\Phi_{fl} = 0.12-0.33$) and are strongly quenched and substantially red-shifted upon protonation (λ_{max} ca. 550 nm, $\Phi_{fl} = 0.010-0.045$). **4**−**5** are 2,6-dimethoxyphenylphenanthrolines with faint luminescence in both the basic and acid form. **6**−**9** are various unsymmetric aryl-substituted-phenanthrolines and their relatively strong fluorescence (λ_{max} ca. 400 nm, $\Phi_{fl} = 0.08-0.24$) is red-shifted and substantially enhanced following protonation (λ_{max} ca. 475 nm, $\Phi_{fl} = 0.16-0.50$). The markedly different trends in the electronic absorption and fluorescence spectra are rationalized by means of both time-dependent Hartree−Fock and density functional theory by using hybrid functionals to assign the excited states. Interestingly, protonation of **1**−**9** also occurs in spin-coated films simply exposed to vapors of acid, and the reaction can be signaled by the color tuning of the emission signal (vapoluminescence). This observation makes substituted phenanthrolines potential candidates as proton sensors also in the solid phase.

1. Introduction

Luminescent sensors for the detection of various chemically, biologically, and environmentally relevant species are attracting a great deal of attention.[1−13] According to the generally favored design, the sensor is made of three components: (i) a signaling unit involved in light absorption and emission, (ii) a receptor module responsible for the binding of the analyte, and (iii) a connecting unit that allows for electronic communication between the other two components.[14] Despite a multitude of powerful luminescence sensors developed in recent decades, it has become evident that the simple intensity modulation of the sensor's luminescence by the analyte, i.e., either increase or decrease of the emission intensity, is less reliable than a ratiometric analysis involving assessment of the changes in the ratio of emission intensities at two different wavelengths. Hence, the assessment of new strategies for rational or phenomenological design of ratiometric luminescent sensors continues to be of paramount importance.[15] Recent years have witnessed a steady flow of new pH responsive luminescent sensors, either organic molecules or coordination compounds,[16−19] with some of them operating on the ratiometric evaluation at two emission wavelengths.

1,10-phenanthroline (phen) was identified 40 years ago as a luminescent heterocyclic system. This molecule and its substituted derivatives represent a very popular class of chelating agents for metal cations.[20−22] However, some intrinsic properties of phenanthroline-type ligands (e.g., structural rigidity and luminescence) also make them attractive as analytical probes, e.g., in proton and cation sensing[16,23−27] or DNA intercalation and groove binding.[28] Suitably engineered phenanthroline ligands can even operate as elementary molecular machines simply by varying the ambient acid concentrations.[29,30] Interestingly, phen exhibits a pH-dependent shifting of the fluorescence maximum allowing the calculation of successive dissociation constants of the protonated species in the excited state.[31−34] The tuning of the absorption and luminescence properties of several substituted phenanthrolines upon protonation has been discussed in the last two decades;[16,23,35,36] however, to the best of our knowledge, a systematic investigation of these trends as a function of the substituents on the chelating core has not yet been reported. In this paper we focus our attention on nine 2,9-aryl-substituted phenanthrolines (**1**−**9**), readily prepared in one- or two-step syntheses, in which the aryl residues are systematically modified or even removed, also with the aim of altering the molecular symmetry. Detailed ^{1}H NMR, UV−vis absorption, and luminescence investigations of **1**−**9** have been carried out as a function of proton concentration in organic solvents and the related spectroscopic trends correlate with the chemical functionalization of the phenanthroline core. These trends are also rationalized with the aid of time-dependent density functional (TDDFT) and Hartree−Fock (TDHF) calculations, which contribute to enlighten the origin of the electronic

* To whom correspondence should be addressed. E-mail: armaroli@isof.cnr.it; schmittel@chemie.uni-siegen.de.
† CNR-ISOF, Bologna.
‡ University of Siegen.

10.1021/jp0723766 CCC: $37.00
Published on Web 07/24/2007

CHART 1: Symmetrically and Unsymmetrically Aryl-Substituted Phenanthrolines 1−9

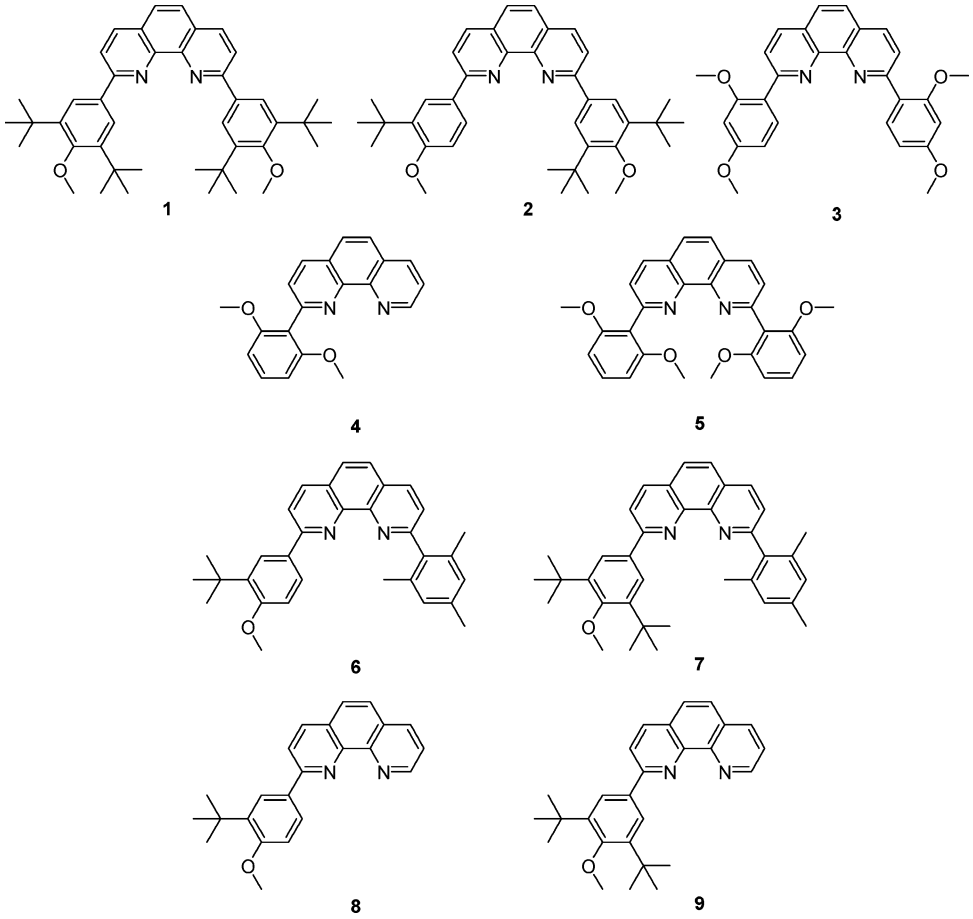

excitations, particularly of the protonated forms. Interestingly, it is shown that substituted phenanthrolines can be profitably exploited as pH responsive luminescent materials, as well as sensors for ratiometric assessment even in solid matrices.

2. Experimental Section

2.1. Synthesis. All compounds were characterized by ^{1}H and ^{13}C NMR, ESI MS, IR, and elemental analysis. ^{1}H NMR and ^{13}C NMR were measured on a Bruker Avance 400 (400 MHz) unless specified otherwise. ESI MS spectra were measured on a LCQ Deca Thermo Quest instrument. Typically, 25 scans were accumulated for each spectrum. The synthesis of compounds **1**, **4**, **5**, **7**, and **9** has been described already in the literature.[37,38] The novel compounds (**2**, **3**, **6**, and **8**) have been prepared according to known aryl lithium addition protocols described earlier.[39] Their characterization data sheets are provided in the Supporting Information.

2.2. Steady-State Absorption and Luminescence. Absorption spectra were recorded with a Perkin-Elmer λ40 spectrophotometer. Emission spectra were obtained with an Edinburgh FLS920 spectrometer (continuous 450 W Xe lamp), equipped with a Peltier-cooled Hamamatsu R928 photomultiplier tube (185−850 nm). Emission quantum yields were determined according to the approach described by Demas and Crosby[40] using quinine sulfate ($\phi_{em} = 0.546$ in air-equilibrated acid water solution, 1 N H_2SO_4)[41] as standard.

2.3. Time-Resolved Luminescence. Emission lifetimes of the species absorbing in the VIS region were determined with the time correlated single photon counting technique, using the above-mentioned Edinburgh FLS920 spectrometer having a laser diode as an excitation source (1 MHz repetition rate, $\lambda_{exc} =$ 407 nm, 200 ps time resolution upon deconvolution) and an Hamamatsu R928 PMT as a detector. Emission lifetimes of the species absorbing in the VIS region were determined with an IBH single photon counting spectrometer equipped with a thyratron gated nitrogen lamp working in the range 2−40 kHz ($\lambda_{exc} \approx$ 337 nm, 0.5 ns time resolution upon deconvolution) and also with a series of nanoleds (IBH) at $\lambda_{exc} =$ 278, 331, and 373 nm; the detector was a red-sensitive (185−850 nm) Hamamatsu R-3237-01 photomultiplier tube. Phosphorescence spectra and related long-lived decay signals (s time scale) were recorded with a Perkin-Elmer LS-50B spectrofluorimeter equipped with a Hamamatsu R928 PMT. Decay analyses were carried out with the manufacturers' software provided with each machine.

2.4. Quantum Chemical Calculations. The calculations used the methods and basis sets implemented in the Gaussian03 software package.[42] First the ground state geometries of the reference molecules were optimized by using the 6-31G* basis set[43] both within density functional theory (DFT),[44] using the Becke three-parameter hybrid functional with the Lee−Yang−Parr correlation corrections (B3LYP),[45−47] and by the ab initio Hartree−Fock (HF) theory,[48] in order to compare the molecular orbital (MO) ordering calculated by the two methods. Afterward all the molecular geometries were optimized by means of the Austin model AM1, using the *tight* option. The singlet excited-state vertical transition energies and oscillator strengths were calculated, using the previously defined basis set, by means of time-dependent density functional theory (TDDFT).[49] The hybrid functionals B3LYP (TD-B3LYP method) and the BHandHLYP half-and-half functional (TD-BHandHLYP method), as implemented within the Gaussian package, were employed. This last contains 50% of HF exchange in its functional, and is

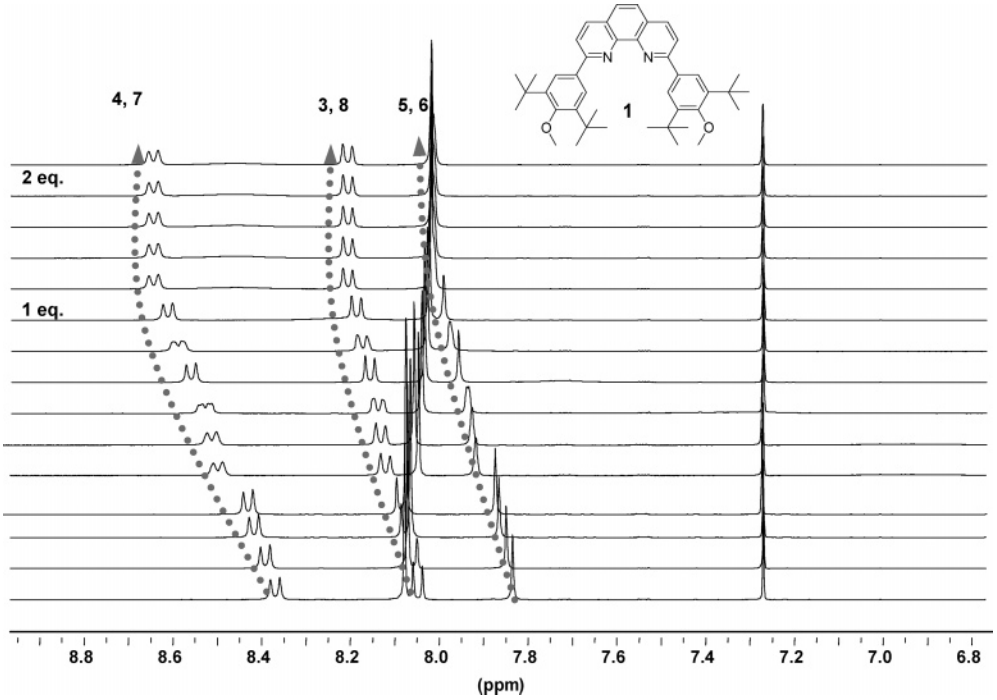

Figure 1. ^{1}H NMR titration of a 0.05 M solution of phenanthroline **1** against TFA in $CDCl_3$.

expected to be more adequate than the first in case of intramolecular charge-transfer states.[50] For comparison, time-dependent Hartree−Fock (TDHF) calculations were also performed.

3. Results and Discussion

3.1. Synthesis. 1−9 (Chart 1) have been prepared along a well-established protocol by the successive addition of the aryl lithium species to the parent or monosubstituted phenanthroline.[39] All compounds were characterized by ^{1}H and ^{13}C NMR, ESI MS, IR, and elemental analysis. Compounds **2**, **3**, **6**, and **8** have been prepared for the first time (see experimental methods), while **1**, **4**, **5**, **7**, and **9** were reported earlier.[37,38]

3.2. ^{1}H NMR Titrations. The response of phenanthrolines **1**−**9** to acid was tested by titrating ca. 0.05 M solutions of the phenanthrolines against TFA in $CDCl_3$. In general, on addition of TFA, the signals of the phenanthrolines displayed marked downfield shifts. On the basis of the analyses of the shifts in the ^{1}H NMR spectra of basic and protonated forms of **1**−**9**, several kinds of chemical shift patterns have been found upon acid addition, as detailed below. Aliquot-wise titrations were performed on phenanthrolines **1**, **4**, **7**, and **9** to obtain more information.

*Phenanthrolines **1**, **3**, and **5**.* These molecules displayed distinct downfield shifts in the two doublets corresponding to protons 4-H, 7-H and 3-H, 8-H upon addition of 1 equiv of TFA. No further characteristic changes were observed upon addition of the second equivalent of TFA. Aliquot-wise titration of **1** with TFA exhibited a linear correlation of the proton shifts with the amount of acid until 1 equiv of TFA was added. Subsequent addition of aliquots of TFA produced very little change (Figure 1).

The behavior of **1**, **3**, and **5** is consistent with a single protonation event (Scheme 1) leading to downfield shifts in all phenanthroline protons. The very minor changes upon addition of the second equivalent of TFA suggest that, under the experimental conditions adopted, a second protonation event is not possible. Apparently, the second protonation requires a stronger acid than TFA. The spectra observed (Figure 1) suggest fast shuttling of the proton between both nitrogens on the NMR time scale, producing an averaged spectrum of the adduct as depicted in Scheme 1.

SCHEME 1: Rapid Shuttling of the Proton between the Two Nitrogens Is Observed upon Protonation of Phenanthrolines 1, 3, and 5

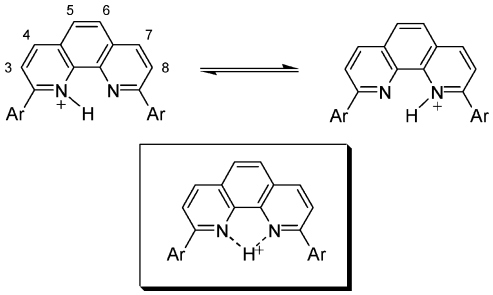

*Phenanthrolines **2**, **6**, and **7**.* Upon addition of 1 equiv of TFA these molecules produced again downfield shifts in the signals of protons 4-H, 7-H and 3-H, 8-H. However, unlike in **1**, **3**, and **5**, the signals of the 4-H and 7-H were observed as two separate doublets. This was observed clearly in a titration of TFA into a solution of **7** in $CDCl_3$ (Figure 2). Subsequent addition of the second equivalent of TFA led to marginal shifts in the phenanthroline signals.

The unsymmetrically substituted diaryl phenanthrolines **2**, **6**, and **7** show a preferential protonation to nitrogen N1 upon addition of the first equivalent of TFA (Scheme 2). This is more evident in **6** and **7** which exhibit two separate doublets for the 4-H and 7-H with the 4-H being more downfield shifted than that of 7-H upon acid addition. However, no further strong shifts are noticed upon addition of the second equivalent.

*Phenanthrolines **4**, **8**, and **9**.* Addition of TFA to the 2-aryl-substituted phenanthrolines **4**, **8**, and **9** induced remarkably strong NMR shifts. Titration of about 1.0 equiv of TFA into a 0.05 M solution of **4** (Figure 3) showed a 0.9 ppm shift in the doublet corresponding to proton 4-H. The doublet corresponding to proton 3-H also exhibited a drastic downfield shift from 7.6

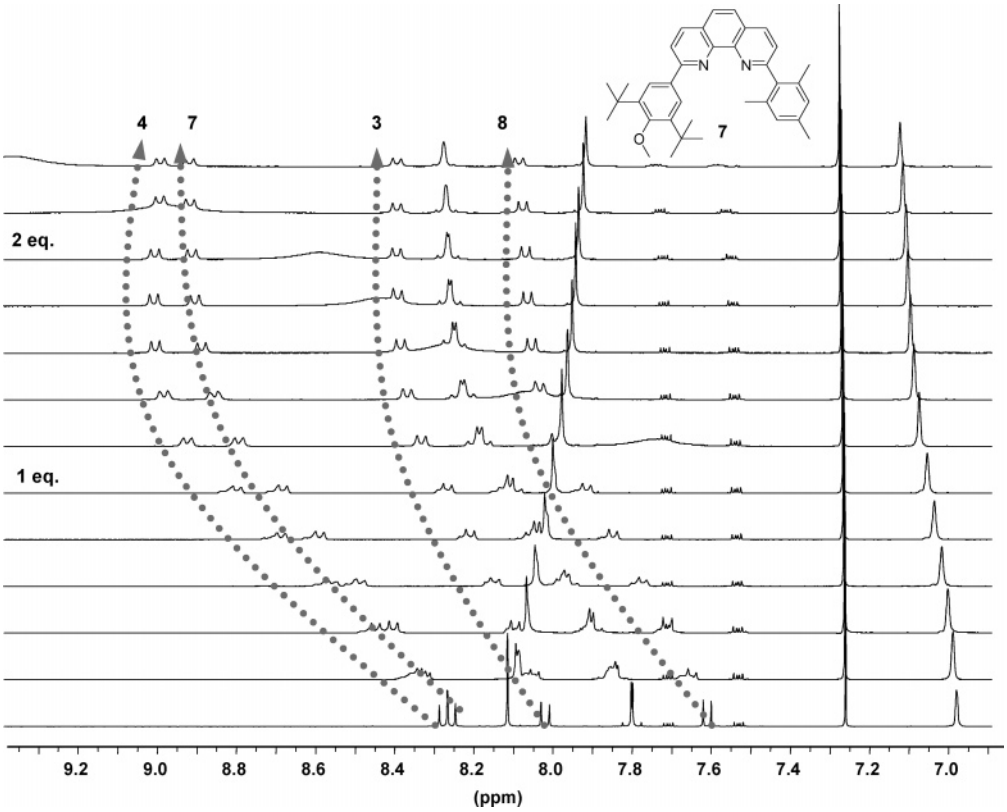

Figure 2. ^{1}H NMR titration of a 0.05 M solution of phenanthroline **7** against TFA in $CDCl_3$.

SCHEME 2: Addition of TFA to Phenanthrolines 2, 6, and 7 Preferentially Leads to Protonation at N1[a]

[a] As before (Scheme 1), rapid shuttling of the proton between nitrogens N1 and N10 is observed

to 8.6 ppm. However, no shifts whatsoever were noticed in the signal corresponding to the 9-H, while a marginal downfield shift was noted in the signal of 7-H. Upon further aliquot addition to 2 equiv no other changes were discernible.

The development of the signals in **4** points to an initial protonation of N1. Most clearly this is evidenced from the unshifted doublet of 9-H. Surprisingly, addition of the second equivalent and further aliquots provided no subsequent changes.

Upon titration of ca. 1.0 equiv of TFA to a 0.06 M solution of **9** (Figure 4), protons 7-H and 9-H displayed a downfield shift of 0.45 ppm, while 4-H showed only a 0.05 ppm downfield shift. Addition of ca. 2.0 equiv of TFA led to further changes. The 9-H displayed no further downfield shifts and beyond 1.5 equiv added, gradually shifted 0.15 ppm upfield. The 7-H shifted further downfield (about 0.7 ppm when compared to parent phenanthroline **9**). The 4-H also displayed a marginal downfield shift of 0.15 ppm. Further addition of up to ca. 30 equiv of TFA led to very little response in the NMR.

For **8** and **9** stronger downfield shifts are noticed for 9-H and 7-H than for 4-H. This points to an initial protonation of the more basic N10 of the phenanthroline.[51]

In summary, the monoaryl-substituted phenanthrolines **4**, **8**, and **9** display distinct evidence of different basicity of N1 and N10. From the development of the signal corresponding to proton 9-H, it can be assumed that the protonation in **4** is completely confined to N1 upon addition of the first equivalent. However, in **9**, despite the fact that protonation at N1 seems to be preferred due to the nearby electron-rich aryl substituent, the proton ends up on N10, most likely due to better solvation (thermodynamic) stabilization of the unshielded $\mathbf{9}\cdot\mathbf{H}_{N10}^{+}$. When more than 1 equiv of acid is available, then protonation at N1 triggers concomitant deprotonation at N10, leading to proton shuttling between N1 and N10 and thus a longer dwelling of the proton on N1. The marked upfield shift of proton 9-H upon addition of the second equivalent substantiates this interpretation. The two trends observed for **4** and **8**−**9** are depicted in Scheme 3.

3.3. Computational Study: The Reference Molecules 2-Phenyl-1,10-phenanthroline (10) and 2,9-Diphenyl-1,10-phenanthroline (11). The modeling of **1**−**9** for the rationalization of their photophysical behavior is accomplished through TDDFT, which nowadays represents a powerful tool for investigating ground and excited states of increasingly large molecules with a fairly high level of accuracy, although TDDFT applicability limitations have been widely discussed in the literature, as recently reviewed by Dreuw and Head-Gordon.[52] In fact, it is known that TDDFT usually gives excellent approximations to excitation energies and estimates the energy differences of valence states with better accuracy than HF theory,[53,54] but its usage becomes critical for charge transfer states.[55] However, DFT-based methods have been criticized for the treatment of the ground state of phenanthrene-like systems[56]

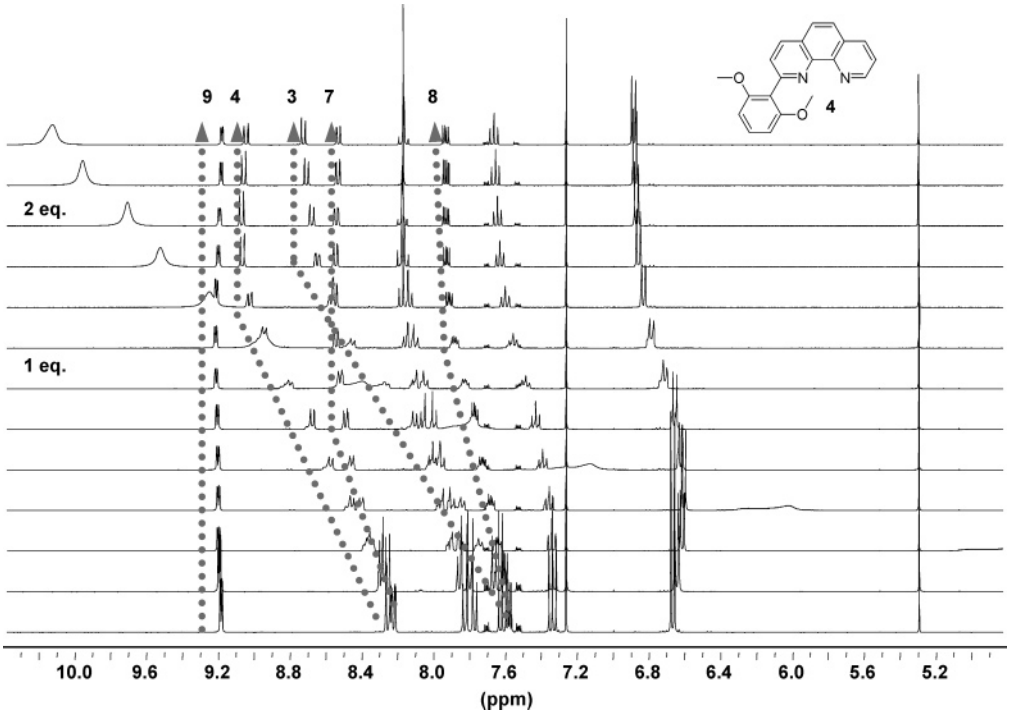

Figure 3. ^{1}H NMR titration of a 0.05 M solution of phenanthroline **4** against TFA in $CDCl_3$.

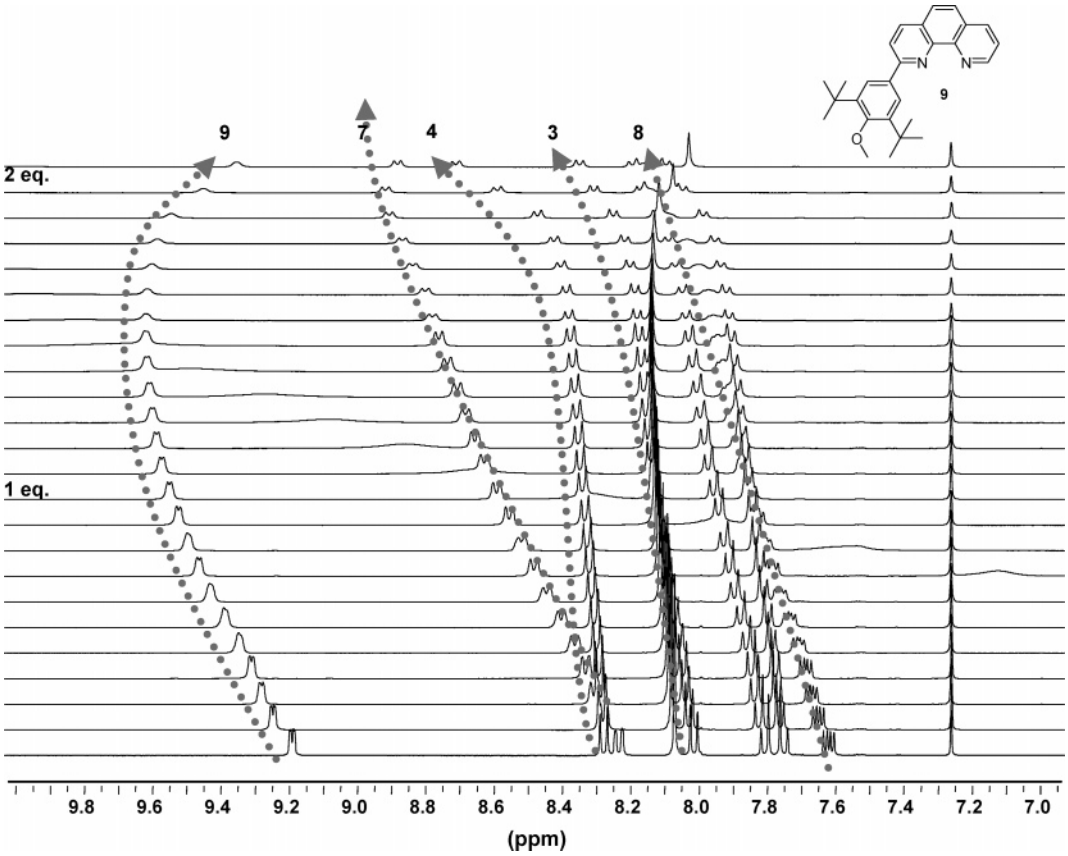

Figure 4. ^{1}H NMR titration of a 0.06 M solution of phenanthroline **9** against TFA in $CDCl_3$.

and, indeed, in the case of pristine 1,10-phenanthroline, they do not reproduce the correct ordering of LUMO and LUMO+1, both of b_1 symmetry in C_{2v},[57] whereas ab initio HF calculations succeed.[58] The whole family of our systems **1**−**9** is made up of aryl-substituted molecules and it is interesting to verify whether DFT is adequate to describe their ground state. Thus we have made computational investigations on **10** and **11**[23] (Chart 2), in which the whole aromatic skeleton is unsubstituted. **10** and **11** can be taken as suitable references, and the results may be compared with those of pristine 1,10-phenanthroline.

Aryl addition to the 2 and 9 position of the phenanthroline core, as in **10** and **11**, can affect the relative energies of LUMO and LUMO+1 orbitals and favor the stabilization of the $\pi^*(a_2)$ MO.[59] Indeed this result is obtained computationally and is

SCHEME 3: Different Behavior of Phenanthrolines 4 vs 8−9 upon Protonation[a]

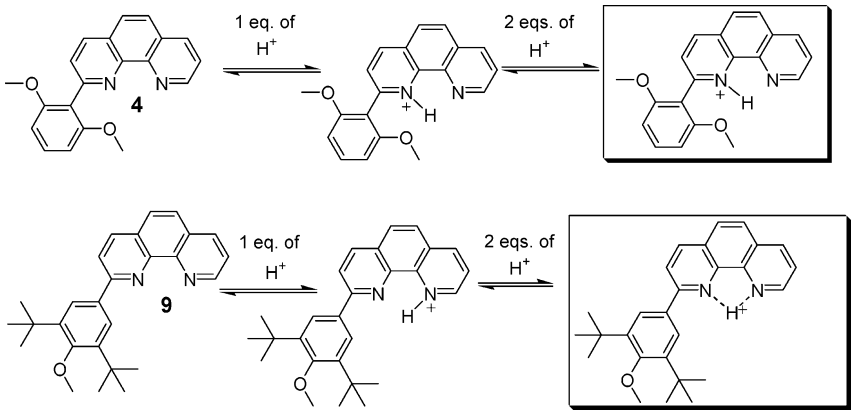

[a] **9** (and **8**) show initial protonation at N10 with one aliquot of TFA and rapid equilibration in the presence of two aliquots of acid.

CHART 2: The Reference Molecules 10 and 11 Used as Reference in the Computational Study

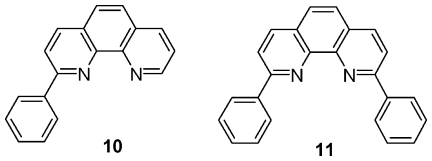

represented in Figure 5,[60] where the MOs of the parent 1,10-phenanthroline (phen) are compared with those of **10** and **11** calculated by both DFT and HF methods.

As a consequence of the LUMO switching, in the case of **10** and **11**, the first excited state is expected to be mainly characterized by a π (b_1) → π^*(a_2) transition, hence correlating with a $^1B_2$ excited state. Protonation of these compounds produces charged species and deeply modifies their MOs as shown in Figure 6[60] for the monoprotonated forms.

It should be pointed out that both the HOMO and HOMO-1 of **10**·$\mathbf{H}_{\mathbf{N10}}^+$ and **11**·$\mathbf{H}^+$ have the electronic clouds localized on different molecular fragments with respect to their LUMO, hence they give rise to weak intramolecular charge-transfer

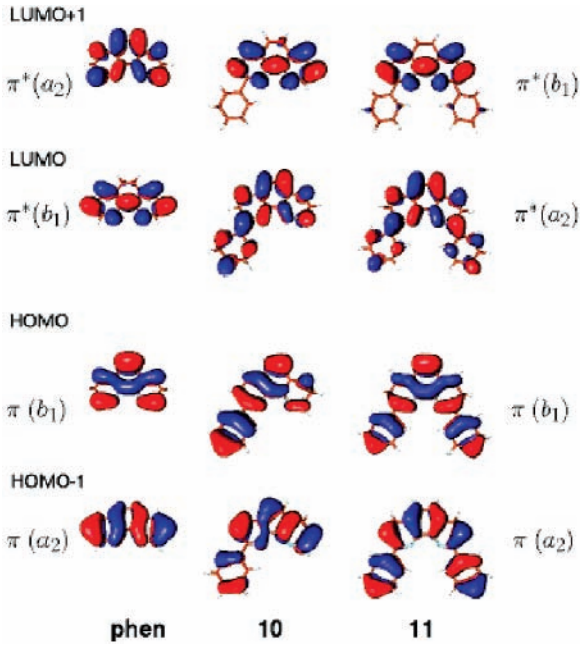

Figure 5. Comparison among the actual frontier orbitals of 1,10-phenanthroline (phen) and those calculated for **10** and **11** by both HF and DFT, using 6-31G* basis set.

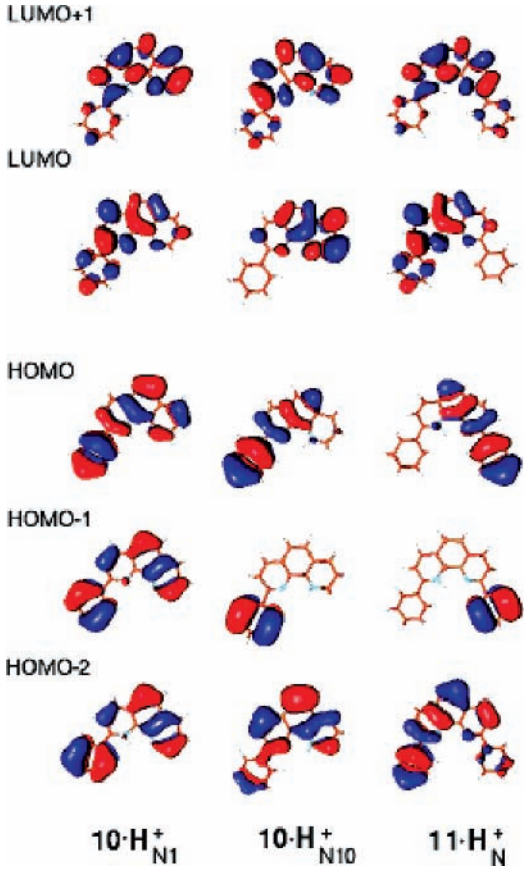

Figure 6. Comparison among the MOs of the monoprotonated forms of **10** and **11** calculated by B3LYP.

transitions, with a significant contribution to the spectral intensity arising from HOMO-2 → LUMO excitations. Therefore, particular attention has to be paid to the choice of the TDDFT method employed, which must be able to properly account for the actual intramolecular charge-transfer transitions. An attempt to overcome this problem was recently suggested by means of hybrid *half-and-half* functionals,[50] such as TD-BHandLYP.

In Table 1 the wavelength and oscillator strength of the transitions to the first two excited states of **10**, **11**, and their protonated forms, calculated by TD-B3LYP and TD-BHandLYP TDDFT methods, are compared with those of TDHF. For **10** the first two excited states are calculated nearly degenerate by both TDDFT methods, while they are better separated (5−7 nm vs 12 nm) in **11**, indicating further stabilization of the

TABLE 1: 10 and 11, along with Their Protonated Compounds: Excited-State Transition Wavelengths (λ) and Oscillator Strengths (f_{osc}) Calculated by (a) TD-B3LYP, (b) TD-BHandHLYP, and (c) TDHF Methods, Using the 6-31G* Basis Set for the Planar Conformers

		10		**10·H$^+_{N1}$**		**10·H$^+_{N10}$**		**10·H$_2^{2+}$**	
	$^1S_0 \rightarrow {}^1S_n$ n	λ	f_{osc}	λ	f_{osc}	λ	f_{osc}	λ	f_{osc}
a	1	330	0.0981	377	0.2655	503	0.0077	471	0.0552
	2	325	0.3314	350	0.1048	434	0.0010	464	0.0308
b	1	292	0.3626	329	0.4459	374	0.0162	371	0.2944
	2	285	0.1368	301	0.0707	314	0.2643	344	0.0150
c	1	268	03285	286	0.5859	287	0.0264	304	0.5724
	2	252	0.0268	264	0.0022	270	0.1903	268	0.1443

			11		**11·H$^+_{N1}$**		**11·H$_2^{2+}$**	
	$^1S_0 \rightarrow {}^1S_n$ n	sym	λ	f_{osc}	λ	f_{osc}	λ	f_{osc}
a	1	B_2	353	0.3851	480	0.0113	440	0.2364
	2	A_1	341	0.0113	408	0.0039	426	0.0181
b	1	B_2	309	0.4961	363	0.0450	366	0.5815
	2	A_1	297	0.0285	323	0.4300	343	0.1830
c	1	B_2	295	0.3719	287	0.4347	304	0.5724
	2	A_1	272	0.0767	278	0.1293	268	0.1443

LUMO with respect to LUMO+1 due to the second aryl addition. Apart from the TD-B3LYP results of **10** and **10·H$_2^{2+}$**, in all cases but that of **10·H$_{N10}^+$**, the first excited state has a large oscillator strength, and the calculated transition energies are markedly red-shifted for all the protonated forms with respect to **10**. Unfortunately, no experimental data are presently available for the electronic transitions of **10** and its protonated cations, but a sample test of the calculated properties will be performed later on, when discussing the phenyl-substituted compounds **4**, **8**, and **9**. Contrary to what happens to **11** and **11·H$_2^{2+}$**, no intense first excited-state transitions are calculated for **11·H$^+$** by both TDDFT methods. The comparison with the recorded absorption spectra of **11** in CH_2Cl_2 solution[23] confirms the correctness of the calculated trend for the transition energies obtained by both TDDFT methods. In fact the fluorescence data (λ_{max} = 362 nm, ϕ = 0.16 for **11**, and λ_{max} = 483 nm, ϕ = 0.077 for **11·H$^+$**)[23] are substantially reproduced by the calculated oscillator strengths. The presence of the diprotonated species **11·H$_2^{2+}$** should manifest itself through a fairly intense absorption, substantially red-shifted with respect to its basic form, but it has not been observed experimentally. This confirms the conclusion previously drawn, i.e., in acidic environment the emitting state belongs to the monoprotonated form of **11**.

Addition of substituents to the aryl groups in **1**−**9** (Chart 1) tunes the electronic properties relative to **10** and **11** so as to enhance, decrease, or even cancel the transition intensities as a function of the substitution pattern, as observed experimentally (see below). It must be mentioned that the comparison of the calculated properties with the experimental data helped to elucidate the origin of the optical properties of the investigated compounds. At the same time it evidenced potentialities and limits of different computational methods allowing the selection of those better suited for the description of substituted phenanthrolines. Details on the calculated results of compounds **1**−**9** and their protonated forms, along with a brief comment, are included in the Supporting Information.

3.4. Photophysical Properties and Acid Titrations at Room Temperature. For the sake of clarity, the presentation of the electronic absorption and emission spectra of **1**−**9** in solution will be split into four parts, dealing with molecules having similar chemical structures and, accordingly, similar photophysical behavior.

*Compounds **1**−**3**.* These compounds have two *p*-anisyl substituents at the phenanthroline core. Such a feature is known to dramatically affect UV−vis absorption and emission spectra

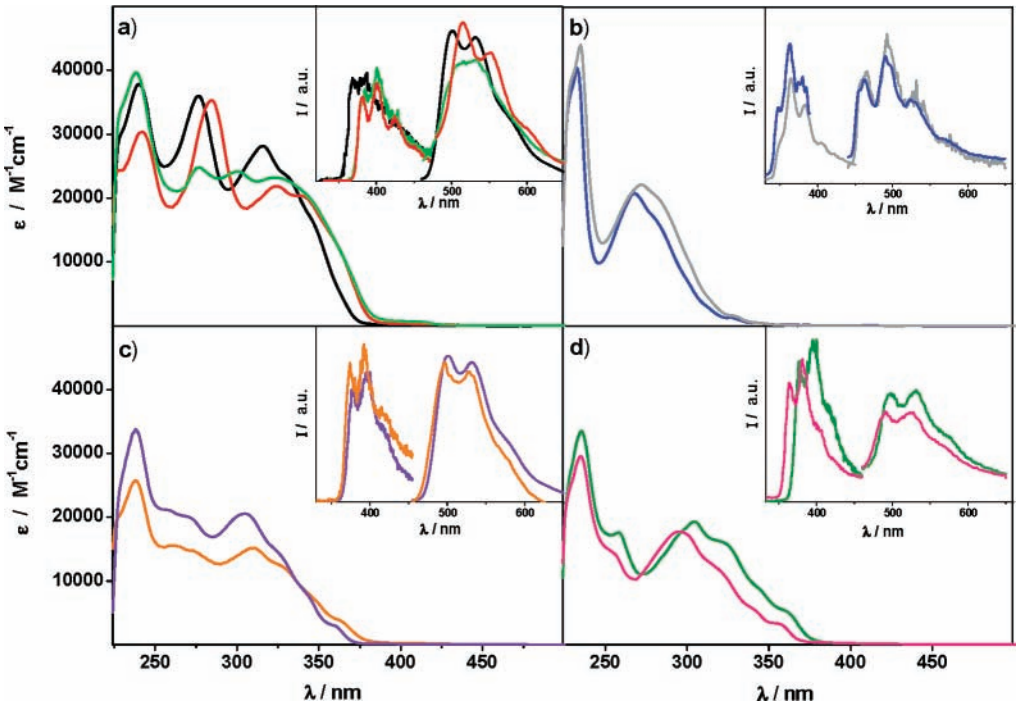

Figure 7. (a) Absorption spectra of **1** (black), **2** (red), and **3** (green) in CH_2Cl_2 at 298 K. Inset: Fluorescence (left) and phosphorescence (right) of **1** (black), **2** (red), and **3** (green) (λ_{exc} = 280 nm) in CH_2Cl_2 at 77 K. (b) Absorption spectra of **4** (blue) and **5** (gray) in CH_2Cl_2 at 298 K. Inset: Fluorescence (left) and phosphorescence (right) of **4** (blue) and **5** (gray) (λ_{exc} = 280 nm) in CH_2Cl_2 at 77 K. (c) Absorption spectra of **6** (orange) and **7** (violet) in CH_2Cl_2 at 298 K. Inset: Fluorescence (left) and phosphorescence (right) of **6** (orange) and **7** (violet) (λ_{exc} = 280 nm) in CH_2Cl_2 at 77 K. (d) Absorption spectra of **8** (olive) and **9** (pink) in CH_2Cl_2 at 298 K. Inset: Fluorescence (left) and phosphorescence (right) of **8** (olive) and **9** (pink) (λ_{exc} = 280 nm) in CH_2Cl_2 at 77 K.

TABLE 2: Luminescence Properties of 1−9 in CH_2Cl_2

	298 K $^1\pi\pi^*$			77 K $^1\pi\pi^*$	77 K $^3\pi\pi^*$	
	$\lambda_{max}{}^a$ (nm)	$\Phi_{em}{}^b$	τ^c (ns)	$\lambda_{max}{}^a$ (nm)	$\lambda_{max}{}^a$ (nm)	τ^d (s)
1	393	0.12	1.8	368	500	1.1
2	404	0.26	1.8	381	514	0.8
3	408	0.33	1.6	384	516	1.0
4	394	0.007	<0.1[e]	347	491	1.4
5	374	0.0005	<0.1[e]	347	493	1.7
6	398	0.12	1.5	374	497	1.1
7	391	0.08	1.0	374	497	0.9
8	398	0.24	2.0	378	499	1.0
9	388	0.11	1.2	365	492	1.0

[a] Emission maxima from spectra corrected for the instrumental response. [b] Fluorescence quantum yields in air-equilibrated solutions. [c] Excited-state singlet lifetimes in air-equilibrated solutions ($\lambda_{exc} = 278$ nm). [d] Excited-state triplet lifetimes in air-equilibrated solutions ($\lambda_{exc} = 280$ nm). [e] Ultrashort and below instrumental resolution.

of 2,9-di-*p*-anisyl-1,10-phenanthroline (dap) compared to those of the parent molecules 1,10-phenanthroline or 2,9-diphenyl-1,10-phenanthroline (**11**).[23] The electronic absorption spectra of **1**−**3**, characterized by the typical intense π,π^* transitions of substituted phenanthrolines, are reported in Figure 7a. As for **11**, the first excited state is assigned to B_2 symmetry (Table S2, Supporting Information). Transitions to this state are polarized along the long molecular axis of the phenanthroline core and have large calculated oscillator strengths.

The spectral shapes of **1** and **2** are fairly similar to those of dap,[23] whereas addition of one extra methoxy group in **3** implies marked spectral changes. Comparison of the experimental data with the TD-B3LYP calculated wavelength maxima and oscillator strengths, assuming coplanarity of the phenanthroline and phenyl units, suggests that the observed blue shift and lower intensity of **1** with respect to **2** and **3** originate from a less planar conformation due to steric hindrance of the second *tert-butyl* substituent, which is preserved also in the excited state. Upon light excitation, **1**−**3** show a strong fluorescence band around 400 nm (Table 2), which is assigned to the lowest $^1\pi\pi^*$ level. The corresponding singlet lifetime is slightly shorter than 2.0 ns. Absorption and fluorescence spectra and singlet lifetimes of **1**−**3** (as well as of **4**−**9**) are largely unaffected in the more polar solvent acetonitrile, whereas fluorescence quantum yields tend to be lower (Table S1, Supporting Information).

Addition of increasing amounts of trifluoroacetic acid (TFA) to 5 μM solutions of **1**−**3** in CH_2Cl_2 causes remarkable changes in the absorption spectra of **1**−**3** (Figure 8, as well as Figures S1 and S2 in the Supporting Information). A single family of neat isosbestic points is maintained throughout the titration, which are fully reversible upon addition of an organic base such as diazabicyclo[4.3.0]non-5-ene (DBN). The observed reversible spectral changes suggest that equilibrium 1 is established in the ground state between **1**−**3** and the corresponding monoprotonated forms **1**·H^+−**3**·H^+:

$$\mathbf{n} + \mathbf{BH} \rightleftarrows \mathbf{n}\cdot\mathbf{H}^+ + \mathbf{B}^- \qquad (1)$$

where **n** and **BH** denote **1**−**3** and trifluoroacetic acid, respectively.

Similarly to **11**·H^+, the intense features with maxima around 390 nm in the absorption spectra of **1**·H^+−**3**·H^+ are assigned to transitions to the second and higher excited states by TDDFT (Table S3, Supporting Information).

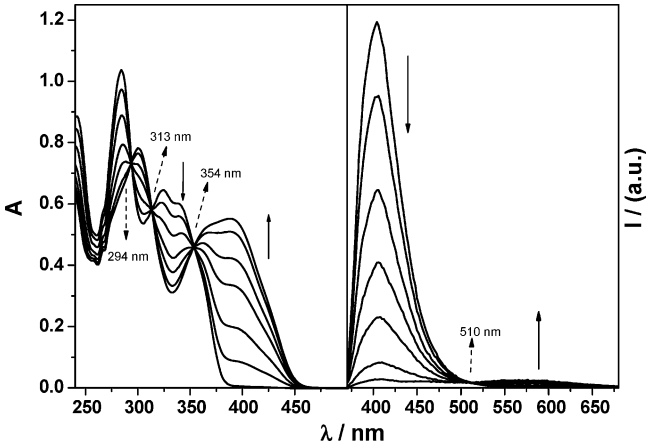

Figure 8. Changes of the absorption (left) and fluorescence spectra (right, $\lambda_{exc} = 313$ nm) of a 5×10^{-6} M solution of **2** in CH_2Cl_2 upon addition of increasing amounts of trifluoroacetic acid (from 0 to 1.5×10^{-5} M). Dashed arrows indicate isosbestic and isoemissive points. The analogous spectroscopic titrations of **1** and **3** are provided as Supporting Information.

TABLE 3: Luminescence Properties of 1·H^+−9·H^+ in CH_2Cl_2

	298 K $^1\pi\pi^*$			77 K $^1\pi\pi^*$	77 K $^3\pi\pi^*$	
	$\lambda_{max}{}^a$ (nm)	$\Phi_{em}{}^b$	τ^c (ns)	$\lambda_{max}{}^a$ (nm)	$\lambda_{max}{}^a$ (nm)	τ^d (s)
1·H^+	600	0.010	4.9	453	501	0.9
2·H^+	596	0.027	6.7	453	521	0.8
3·H^+	578	0.045	8.7	513	541	0.9
4·H^+	498	0.024	3.3	446	490	0.5
5·H^+	490	0.010	3.8	451	488	0.5
6·H^+	474	0.37	4.2	455	510	0.9
7·H^+	475	0.16	4.4	455	502	0.9
8·H^+	474	0.44	4.4	491	518	0.9
9·H^+	478	0.50	4.2	453	497	1.0

[a] Emission maxima from spectra corrected for the instrumental response. [b] Fluorescence quantum yields in air-equilibrated solutions. [c] Excited-state singlet lifetimes in air-equilibrated solutions ($\lambda_{exc} = 407$ nm). [d] Excited-state triplet lifetimes in CH_2Cl_2 rigid matrix at 77 K ($\lambda_{exc} = 280$ nm).

Parallel with absorption changes profound modifications of the fluorescence spectra are observed with a progressive quenching of the blue-violet emission of **1**−**3** and the contemporary rise of a weak and broad emission band with a maximum peaked around 590 nm attributable to **1**·H^+−**3**·H^+ (Table 3 and Figure 8, as well as Figures S1 and S2 in the Supporting Information). Notably, as for **11**·H^+, their first excited-state transitions have an oscillator strength much lower than that of their basic forms. The higher quantum yield determined for the protonated forms of **2** compared to **1** is attributed to the emission from the lowest excited state of **2**·$H_{N1}{}^+$, in agreement with NMR findings.

Despite luminescence intensity variations, the excited-state lifetimes of **1**−**3** and **1**·H^+−**3**·H^+ are constant throughout the titration process, corroborating the reaction scheme described in (1). In addition, excitation spectra of **1**·H^+−**3**·H^+ match the profiles of the corresponding absorption traces at the end of the titration. The equivalents of TFA that are needed to stop the spectral variations for **3** (1.2 ± 0.2) are lower than those for **1** and **2** (3.0 ± 0.2) suggesting that the former is a stronger base.

*Compounds **4** and **5**.* This couple of compounds allows (i) the effect of aryl disubstitution in *ortho* positions to be tested

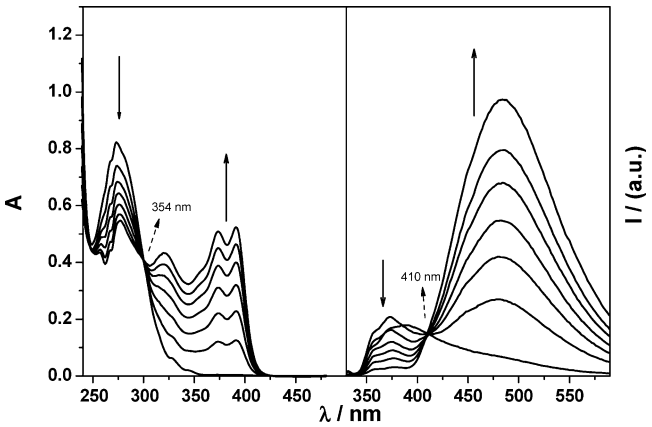

Figure 9. Changes of the absorption (left) and fluorescence spectra (right, $\lambda_{exc} = 354$ nm) of a 5×10^{-6} M solution of **5** in CH_2Cl_2 upon addition of increasing amounts of trifluoroacetic acid (from 0 to 5×10^{-6} M). Dashed arrows indicate isosbestic and isoemissive points. The analogous spectroscopic titration of **4** is provided as Supporting Information.

and (ii) the comparison of 2- (**4**) vs 2,9-aryl (**5**)-substituted systems. The shapes of the absorption spectra of **4** and **5** are rather similar (Figure 7b) and the similarity is maintained throughout the titration process as documented by a single family of isosbestic points in both cases (Figure 9, as well as Figure S3 in the Supporting Information). Both titrations are completed with the same amount of acid (1.0 ± 0.2).

The stronger basicity of **4** and **5**, compared to that of **1**−**3**, can be related to the presence of two methoxy groups on the aryl residue (see above). **4** and **5** are the only two systems of the whole series exhibiting strongly quenched fluorescence in the basic form at room temperature ($\Phi_{fl} < 1\%$, $\tau < 100$ ps, Table 1). Upon protonation, the emission signal is substantially increased and also blue-shifted compared to that of **1**·H^+−**3**·H^+ (Figure 7, as well as Figure S3 in the Supporting Information). The formation of **4**·H^+ and **5**·H^+ according to (1) is also supported by the following experimental observations: (i) the spectral variations observed during the titrations of **4** and **5** are fully reversible upon addition of an organic base; (ii) the excitation spectra taken at the end of the titration processes match the corresponding absorption profiles; and (iii) despite emission intensity variations, the excited-state luminescence lifetimes are constant throughout the titration process. Observations i−iii are also found for **6**−**9**, presented below.

The anomalous behavior of **4** and **5** with respect to the other examined compounds can be attributed to oxygen−nitrogen electron repulsion effects and/or to the N−H hydrogen bond involving the methoxy substituent. Both of these effects tend to hinder the planarity of these molecules (Figure 10) and this correlates with the fact that the absorption spectra of **4** and **5** are markedly blue-shifted when compared to those of the other compounds (Figure 7).

Interestingly, TD-B3LYP calculations on the conformers of **4** and **5** (Table S4, Supporting Information) point to a rather intense $\pi-\pi^*$ first excited-state transition with a negligible calculated energy shift among them (1−2 nm). The weak emission detected for **4** and **5** points to a decay process from an excited state of different nature. In fact, a $^1S_1$ $\sigma-\pi^*$ excited state with very low oscillator strength ($f_{osc} = 0.0007$) is calculated for the planar conformer of **4** by TD-B3LYP, in agreement with the low observed emission quantum yield (Table 2). Comparison with the experimental data suggests that **4** and **5** undergo a significant variation of the phenanthroline/phenyl torsional angles during relaxation of the excited state, in which a more planar conformation is favored due to more extensive conjugation among the molecular fragments of the LUMO (skeleton of the reference compound shown in Figure 5). Out of the two molecules, **4** can quite easily adopt a planar conformation, which destabilizes its MO(σ) and favors the $^1S_1$ $\sigma-\pi^*$ excited-state decay. On the contrary, steric hindrance of two aryl substituents inhibits planarization of **5**. Test calculations performed on **5** by means of the TD-B3LYP method, considering different geometries, point to a strained structure having only one aryl coplanar with the phenanthroline fragment. This stabilizes a $^1S_1$ $\sigma-\pi^*$ excited state having a low calculated oscillator strength ($f_{osc} = 0.0020$).

*Compounds **6** and **7**.* The key feature of these phenanthrolines is the combination of a 2-methoxyaryl with a 9-mesityl unit, resulting in unsymmetrically substituted structures. The absorption and luminescence spectra of **6** and **7** are very similar in both the basic and acid form (Figure 11, as well as Figure S4 in the Supporting Information). Protonation is completed upon addition of 3.0 ± 0.2 equiv of acid, as observed for **2,** which, according to NMR data, analogously undergoes protonation of N1 first.

The lower basicity of N10 compared to N1 in **6** and **7** might be related to steric effects of the nearby *o*-methyl substituent as derived from the calculated geometry, which also shows that N10 interacts with the nearby methyl hydrogen. TD-B3LYP calculations (Table S2, Supporting Information) show a substantial similarity between the calculated energies and intensities of **6** and **7**, in agreement with their absorption spectra.

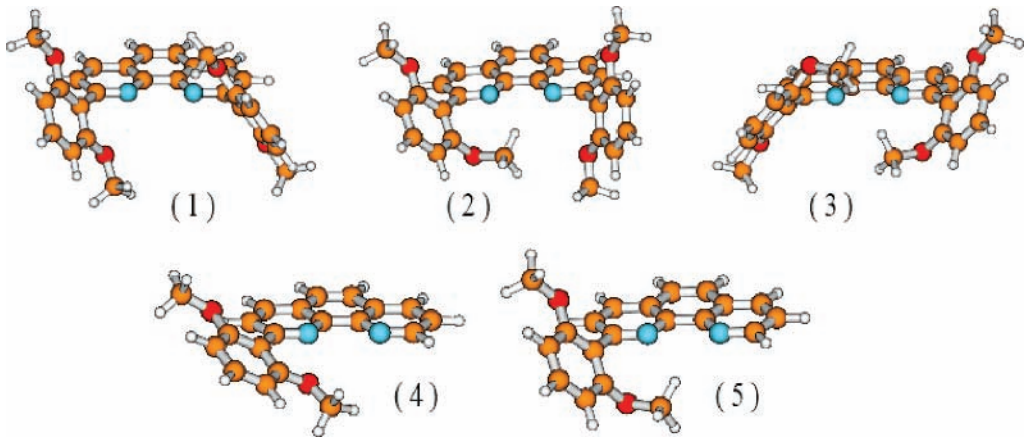

Figure 10. Stable conformers of **4** [(4) and (5)] and **5** [(1), (2), and (3)] obtained by geometry optimization with B3LYP. (1) and (4) are due to electronic repulsion of the N and O atoms, while (2), (3), and (5) show the interaction of a methoxy hydrogen with both nitrogens.

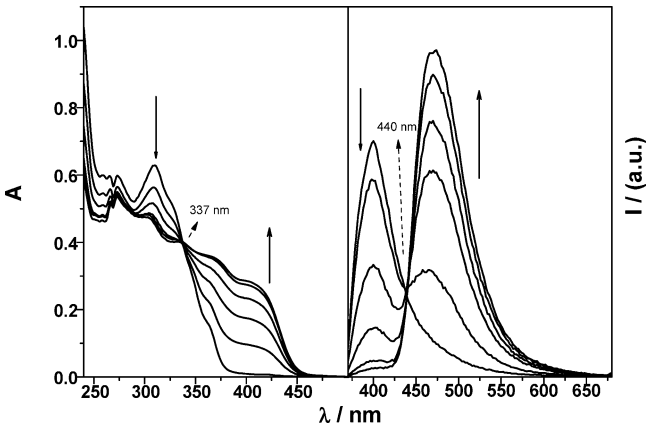

Figure 11. Changes of the absorption (left) and fluorescence spectra (right, $\lambda_{exc} = 337$ nm) of a 5×10^{-6} M solution of **6** in CH_2Cl_2 upon addition of increasing amounts of trifluoroacetic acid (from 0 to 1.5×10^{-5} M). Dashed arrows indicate isosbestic and isoemissive points. The analogous spectroscopic titration of **7** is provided as Supporting Information.

The most relevant feature of **6** and **7** is the enhancement of the luminescence quantum yield upon protonation, to be compared with the opposite trend observed for **1**−**3**. The origin of such an intense transition turned out to be difficult to rationalize with TDDFT methods. Only TDHF assigns (Table S5, Supporting Information) a strong transition to the monoprotonated form (N1), which emphasizes the contribution of the excitation arising from the orbital correlated with the HOMO-2 of **11**·H^+ (see Figure 6). On the basis of this method, the lower emission quantum yield observed for **7** with respect to **6** is largely attributed to steric hindrance due to the presence of a second *tert-butyl* group that inhibits planarity also in the $^1S_1$ excited state. The high fluorescence quantum yield of **6** and **7** (up to 0.37) makes them particularly attractive as proton sensors in organic solvents.

*Compounds **8** and **9**.* These molecules lack the mesitylene residue relative to **6** and **7**. This modification leads to a substantial increase of the absorption spectral intensities between 250 and 300 nm (Figure 12). The spectral changes observed during the titration of **8** and **9** with TFA follow a different trend compared to those of **1**−**7**. A single family of clean isosbestic points is observed only up to 0.6 ± 0.1 equiv of acid added and, in parallel, a substantial decrease of the fluorescence band with maximum above 400 nm (basic form) is monitored along with the rise of a red-shifted band attributable to **8**·H^+ and **9**·H^+ (Figure 12, as well as Figure S5 in the Supporting Information).

Afterward, changes in the absorption spectra are observed also upon further addition of acid but clean isosbestic points are no longer detected; meanwhile the fluorescence signal substantially grows. The emission quantum yields of **8** and **9** reach very high values (up to 0.50, Table 3) upon addition of 300−500 equiv of trifluoroacetic acid or just 2 equiv of the much stronger triflic acid CF_3SO_3H. This peculiar behavior of **8** and **9** in acidic CH_2Cl_2 is not easy to rationalize and explanations such as formation of multiple equilibria or photochemical reaction in chlorinated solvents might be invoked.[61] The calculated oscillator strengths of both **8** and **9** (Table S6, Supporting Information) attribute a weak intensity in the case of **8**·H_{N10}^+ and **9**·H_{N10}^+ and very large intensity in the case of **8**·H_{N1}^+ and **9**·H_{N1}^+ for transitions to the first excited state (Table S6 and S7, Supporting Information). Moreover, TDHF also points to the diprotonated cation as the origin of a very intense transition. On the basis of NMR findings, however, we have to assume that even at a very large excess of acid added only monoprotonation occurs. Actually, the same NMR spectrum is recorded in the presence of 100 equiv of TFA or 1 equiv of the much stronger acid CF_3SO_3H (Figure S8, Supporting Information). Even further addition of CF_3SO_3H does not reveal formation of a diprotonated species. From the NMR titrations it seems evident that protonation occurs first at N10. At higher

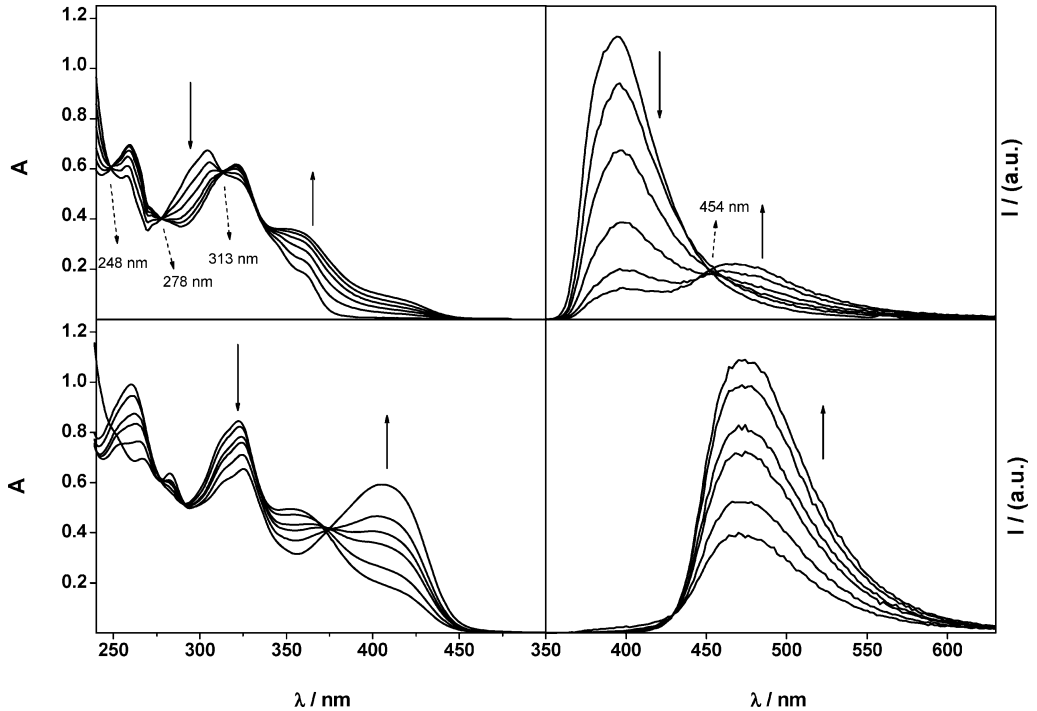

Figure 12. Top: Changes of the absorption (left) and fluorescence spectra (right, $\lambda_{exc} = 313$ nm) of a 5×10^{-6} M solution of **8** in CH_2Cl_2 upon addition of increasing amounts of trifluoroacetic acid (from 0 to 3.0×10^{-6} M). Bottom: Further changes in the absorption and fluorescence spectra ($\lambda_{exc} = 374$ nm) upon addition of acid up to 2.5×10^{-3} M (500 equiv). Dashed arrows indicate isosbestic and isoemissive points. The analogous spectroscopic titration of **9** is provided as Supporting Information.

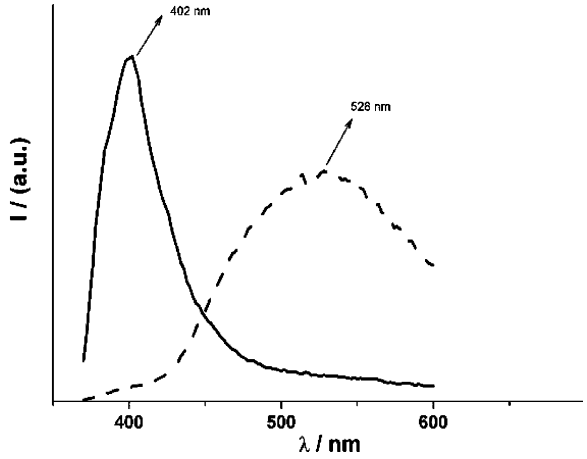

Figure 13. Fluorescence spectra of a thin film of **2** before (full line) and after exposition for 3 s to vapors of trifluoroacetic acid (dashed line).

amounts of acid, however, the 9-H experiences a high field shift, suggesting that the protonated species is now better represented with the proton rapidly shuttling between N10 and N1. As the thermodynamic preference for protonation at N10 should not change with higher acid concentrations, the increased protonation at N1 might be due to a dynamic effect. It is suggested that, with larger amounts of acid, protonation at N1 of **8**·H^+ and **9**·H^+ sets in, leading to immediate deprotonation at N10 and a subsequent shift of the proton from N1 to N10 as required by thermodynamics. The net effect is that protonation is more and more felt at N1. In agreement with this model the emission of solutions of **8** and **9** continuously increases with acid addition (up to 500 equiv).

3.5. Emission Spectra at 77 K and in the Solid State. Luminescence spectra of **1**−**9** and **1**·H^+−**9**·H^+ were also recorded in CH_2Cl_2 rigid matrix at 77 K, and two bands were invariably observed (Figure 7). The intense and short-lived bands of **1**−**9** with maximum below 400 nm (Table 1) is the $^1\pi\pi^*$ fluorescence, slightly blue-shifted compared to room temperature. The red-shifted, structured, and long-lived emission centered around 500 nm is attributed to phosphorescence deactivation from the lowest $^3\pi\pi^*$ level, as discussed previously in similar systems.[23] Passing to **1**·H^+−**9**·H^+, fluorescence bands are red-shifted compared to the basic form at low temperature, but substantially blue-shifted relative to the corresponding room temperature spectra, especially in the case of **1**−**3** (Table 2). In the low-temperature rigid matrix the solvent repolarization around excited states is substantially limited, thus the observed blue shift substantiates the partial charge-transfer character of the $^1\pi\pi^*$ lowest level in 2,9-substituted phenanthrolines proposed previously.[23] By contrast, the position of the phosphorescence spectra of **1**−**9** is negligibly affected upon protonation, and such a small effect on the $^3\pi\pi^*$ levels, compared with that observed for the corresponding singlet excited states, can be attributed to the smaller charge-transfer character of the former level as suggested by spin-correlation arguments.

Phenanthrolines **1**−**9** have been spin coated from dichloromethane solution onto glass substrates (90 nm thick films, polycarbonate matrix 6% w/w). Fluorescence spectra and lifetimes detected under these conditions are very similar to those in fluid solution (Figure 13), showing that the nature of the lowest excited state is unchanged when embedded in the rigid medium. To test the potential of these systems as proton sensors we exposed the spin-coated films to vapors of trifluoroacetic acid for 3 s.

Fluorescence bands detected under these conditions exhibit intermediate spectral positions between those of 298 K fluid solutions and 77 K, as expected in a rigid medium on the basis of the partial charge-transfer character of the related transition (see discussion on 77 K spectra). As an example, in Figure 13 are reported the spectra of **2** and **2**·H^+ spin-coated on glass. The latter exhibits a broad spectrum peaked at 528 nm, to be compared to 596 and 453 nm in room temperature fluid solution and 77 K CH_2Cl_2 matrix. The emission signal was maintained without loss for several days at ambient conditions, suggesting a good stability of the protonated films.

Conclusions

Substituted phenanthrolines and their protonated forms have been extensively investigated in the past.[29] These molecules are photoluminescent and their emission output is substantially tuned in intensity and color depending on the substitution pattern of the phenanthroline core and on the acidity of the environment. We have presented here a systematic study on nine substituted phenanthrolines aiming at the rationalization of these trends with the aid of ^{1}H NMR, UV−vis absorption, and luminescence spectroscopy, along with TDDFT and TDHF computational methods. NMR spectroscopy allowed the determination of the localization of H^+ in the monoprotonated forms showing that, in symmetric systems, the proton is shared between the phenanthroline nitrogens, whereas for asymmetric systems preferential protonation at the N1 or N10 site may occur. The preferential location is dictated by a combination of steric and electronic effects. In the basic forms strong fluorescence is observed for both symmetric (e.g., **1**,**3**) and unsymmetric systems (e.g., **2**,**8**); however, virtually complete switching-off is also detected in some cases (**4**,**5**). Only unsymmetric molecules may originate in strongly emissive protonated forms, particularly when only one *p*-methoxybenzene group is present as a substituent (**6**−**9**); in these cases the fluorescence quantum yield can reach values as high as 50%. Protonation has been investigated in the solid matrix by simple exposition of spin coated films of **1**−**9**. The color of the luminescence signal turned from blue-violet to yellow-green in the presence of TFA, revealing the occurrence of the protonation reaction also in the solid matrix. **1**−**9** have been investigated also by computational methods and the extensive information gained suggests that TDDFT through the B3LYP and BHandLYP hybrid functionals are suitable to investigate the optical behavior of symmetrically substituted phenanthrolines, derived from **11**, in both their basic and protonated forms. For the latter, these methods fail to properly account for intramolecular charge-transfer transitions[55] in the case of unsymmetrically substituted compounds, whereas TDHF succeeds. The experimental findings suggest caution in using hybrid functionals to investigate unsymmetric analogues of **10**, though, based on TD-B3LYP, a reasonable explanation of the anomalous behavior of **4** and **5** can be obtained. The successful combination of experimental and theoretical methods may now allow the design of phenanthroline structures with optimized luminescence performance. Some of them are now under investigation in our laboratories and will be reported in due time.

Acknowledgment. We gratefully acknowledge financial support by the Italian CNR (commessa PM.P04.010, MACOL) and the Deutsche Forschungsgemeinschaft. We are indebted to Christoph Michel and Alvaro Iglesias Gonzalez for experimental help with some of the compounds.

Supporting Information Available: NMR characterization data sheets of **2**, **3**, **6**, **8**, and figures showing absorption and

emission titrations of **1**, **3**, **4**, **7**, and **9** in CH_2Cl_2, luminescence properties of **1**−**9** in CH_3CN, and calculated wavelengths and oscillator strengths of **1**−**9** and their protonated forms for transitions from $^1S_0$ to $^1S_1$ and $^1S_2$, followed by a brief comment. This material is available free of charge via the Internet at http://pubs.acs.org.

References and Notes

(1) deSilva, A. P.; Gunaratne, H. Q. N.; Gunnlaugsson, T.; Huxley, A. J. M.; McCoy, C. P.; Rademacher, J. T.; Rice, T. E. *Chem. Rev.* **1997**, *97*, 1515.

(2) Bargossi, C.; Fiorini, M. C.; Montalti, M.; Prodi, L.; Zaccheroni, N. *Coord. Chem. Rev.* **2000**, *208*, 17.

(3) Valeur, B.; Leray, I. *Coord. Chem. Rev.* **2000**, *205*, 3.

(4) de Silva, A. P.; Fox, D. B.; Huxley, A. J. M.; Moody, T. S. *Coord. Chem. Rev.* **2000**, *205*, 41.

(5) Prodi, L.; Bolletta, F.; Montalti, M.; Zaccheroni, N. *Coord. Chem. Rev.* **2000**, *205*, 59.

(6) Fabbrizzi, L.; Licchelli, M.; Rabaioli, G.; Taglietti, A. *Coord. Chem. Rev.* **2000**, *205*, 85.

(7) Parker, D. *Coord. Chem. Rev.* **2000**, *205*, 109.

(8) Beer, P. D.; Cadman, J. *Coord. Chem. Rev.* **2000**, *205*, 131.

(9) Robertson, A.; Shinkai, S. *Coord. Chem. Rev.* **2000**, *205*, 157.

(10) Keefe, M. H.; Benkstein, K. D.; Hupp, J. T. *Coord. Chem. Rev.* **2000**, *205*, 201.

(11) Ramamurthy, V.; Schanze, K. S., Eds. *Optical sensors and switches*; Marcel Dekker: New York, 2001.

(12) Prodi, L. *New J. Chem.* **2005**, *29*, 20.

(13) Callan, J. F.; de Silva, A. P.; Magri, D. C. *Tetrahedron* **2005**, *61*, 8551.

(14) Fabbrizzi, L.; Poggi, A. *Chem. Soc. Rev.* **1995**, *24*, 197.

(15) Banthia, S.; Samanta, A. *J. Phys. Chem. B* **2006**, *110*, 6437.

(16) Joshi, H. S.; Jamshidi, R.; Tor, Y. *Angew. Chem., Int. Ed.* **1999**, *38*, 2722.

(17) Greiner, G.; Maier, I. *J. Chem. Soc., Perkin Trans. 2* **2002**, 1005.

(18) Higgins, B.; DeGraff, B. A.; Demas, J. N. *Inorg. Chem.* **2005**, *44*, 6662.

(19) Wong, K. M. C.; Tang, W. S.; Lu, X. X.; Zhu, N. Y.; Yam, V. W. W. *Inorg. Chem.* **2005**, *44*, 1492.

(20) Sammes, P. G.; Yahioglu, G. *Chem. Soc. Rev.* **1994**, *23*, 327.

(21) McMillin, D. R.; McNett, K. M. *Chem. Rev.* **1998**, *98*, 1201.

(22) Armaroli, N. *Chem. Soc. Rev.* **2001**, *30*, 113.

(23) Armaroli, N.; De Cola, L.; Balzani, V.; Sauvage, J. P.; Dietrich-Buchecker, C. O.; Kern, J. M. *J. Chem. Soc., Faraday Trans.* **1992**, *88*, 553.

(24) Loren, J. C.; Siegel, J. S. *Angew. Chem., Int. Ed.* **2001**, *40*, 754.

(25) Bencini, A.; Bernardo, M. A.; Bianchi, A.; Fusi, V.; Giorgi, C.; Pina, F.; Valtancoli, B. *Eur. J. Inorg. Chem.* **1999**, 1911.

(26) Aragoni, M. C.; Arca, M.; Demartin, F.; Devillanova, F. A.; Isaia, F.; Garau, A.; Lippolis, V.; Jalali, F.; Papke, U.; Shamsipur, M.; Tei, L.; Yari, A.; Verani, G. *Inorg. Chem.* **2002**, *41*, 6623.

(27) Pina, J.; de Melo, J. S.; Pina, F.; Lodeiro, C.; Lima, J. C.; Parola, A. J.; Soriano, C.; Clares, M. P.; Albelda, M. T.; Aucejo, R.; Garcia-Espana, E. *Inorg. Chem.* **2005**, *44*, 7449.

(28) Hayashi, K.; Akutsu, H.; Ozaki, H.; Sawai, H. *Chem. Commun.* **2004**, 1386.

(29) Armaroli, N. *Photochem. Photobiol. Sci.* **2003**, *2*, 73.

(30) Armaroli, N.; De Cola, L.; Balzani, V.; Sauvage, J. P.; Dietrich-Buchecker, C. O.; Kern, J. M.; Bailal, A. *J. Chem. Soc., Dalton Trans.* **1993**, 3241.

(31) Brinen, J. S.; Rosebrook, D. D.; Hirt, R. C. *J. Phys. Chem.* **1963**, *67*, 2651.

(32) Schulman, S. G.; Capomacchia, A. C. *J. Phys. Chem.* **1975**, *79*, 1337.

(33) Bandyopadhyay, B. N.; Harriman, A. *J. Chem. Soc., Faraday Trans. I* **1977**, *73*, 663.

(34) Schulman, S. G.; Tidwell, P. T.; Cetorelli, J. J.; Winefordner, J. D. *J. Am. Chem. Soc.* **1971**, *93*, 3179.

(35) Dietrich-Buchecker, C. O.; Sauvage, J. P.; Armaroli, N.; Ceroni, P.; Balzani, V. *New J. Chem.* **1996**, *20*, 801.

(36) Armaroli, N.; Ceroni, P.; Balzani, V.; Kern, J. M.; Sauvage, J. P.; Weidmann, J. L. *J. Chem. Soc., Faraday Trans.* **1997**, *93*, 4145.

(37) Kalsani, V.; Schmittel, M.; Listorti, A.; Accorsi, G.; Armaroli, N. *Inorg. Chem.* **2006**, *45*, 2061.

(38) Lüning, U.; Müller, M. *Angew. Chem., Int. Ed. Engl.* **1992**, *31*, 80.

(39) Schmittel, M.; Michel, C.; Wiegrefe, A.; Kalsani, V. *Synthesis* **2001**, 1561.

(40) Demas, J. N.; Crosby, G. A. *J. Phys. Chem.* **1971**, *75*, 991.

(41) Meech, S. R.; Phillips, D. *J. Photochem.* **1983**, *23*, 193.

(42) Frisch, M. J.; et al. *Gaussian 03*, Revision D.02; Gaussian, Inc.: Wallingford, CT, 2004.

(43) Hariharan, P. C.; Pople, J. A. *Theor. Chem. Acc.* **1973**, *28*, 213.

(44) Parr, R. G.; Yang, W. *Density-functional theory of atoms and molecules*; Oxford University Press: Oxford, UK, 1989.

(45) Becke, A. D. *J. Chem. Phys.* **1993**, *98*, 5648.

(46) Lee, C. T.; Yang, W. T.; Parr, R. G. *Phys. Rev. B* **1988**, *37*, 785.

(47) Miehlich, B.; Savin, A.; Stoll, H.; Preuss, H. *Chem. Phys. Lett.* **1989**, *157*, 200.

(48) McWeeny, R. In *Methods of Molecular Quantum Mechanics*; Craig, D. P., McWeeny, R., Eds.; Academic Press: London, UK, 1978.

(49) Stratmann, R. E.; Scuseria, G. E.; Frisch, M. J. *J. Chem. Phys.* **1998**, *109*, 8218.

(50) Dreuw, A.; Weisman, J. L.; Head-Gordon, M. *J. Chem. Phys.* **2003**, *119*, 2943.

(51) Formation of species **9**·H^+ in the course of the proton addition has been discarded on the basis of lacking high-field shifts of the *tert*-butyl groups.

(52) Dreuw, A.; Head-Gordon, M. *Chem. Rev.* **2005**, *105*, 4009.

(53) Savin, A.; Umrigar, C. J.; Gonze, X. *Chem. Phys. Lett.* **1998**, *288*, 391.

(54) Gritsenko, O.; Baerends, E. J. *J. Chem. Phys.* **2004**, *121*, 655.

(55) Grimme, S.; Parac, M. *Chem. Phys. Chem.* **2003**, *4*, 292.

(56) Gonzalez-Luque, R.; Serrano-Andres, L.; Merchan, M.; Fulscher, M. P. *Theor. Chem. Acc.* **2003**, *110*, 224.

(57) Kaim, W. *J. Am. Chem. Soc.* **1982**, *104*, 3833.

(58) Ernst, S.; Vogler, C.; Klein, A.; Kaim, W.; Zalis, S. *Inorg. Chem.* **1996**, *35*, 1295.

(59) Farrell, I. R.; Hartl, F.; Zalis, S.; Mahabiersing, T.; Vlcek, A. *J. Chem. Soc., Dalton Trans.* **2000**, 4323.

(60) Schaftenaar, G.; Noordik, J. H. *J. Comput.-Aided Mol. Des.* **2000**, *14*, 123.

(61) Light irradiation of phenanthroline ligands in air-equilibrated dichloromethane solution leads to absorption spectral changes similar to those observed upon protonation, which are also reversible upon addition of base. However, the extensive absorption and emission changes of **8** and **9** in strongly acid environment have been detected also upon removal of oxygen from the solution and working in a dark room. Accordingly we can exclude that the peculiar luminescence behaviour of **8** and **9** in acidic dichloromethane is related to extensive photochemical degradation.